

# Termination of bottom-up interstellar aromatic ring formation at $C_6H_5^+$

Received: 5 October 2024

G. S. Kocheril <sup>1,2</sup>✉, C. Zagorec-Marks <sup>1,2</sup> & H. J. Lewandowski <sup>1,2</sup>

Accepted: 11 February 2025

Published online: 13 March 2025

 Check for updates

The aromatic molecule benzene is considered to be the essential building block for larger polycyclic aromatic hydrocarbons (PAHs) in space. Despite the importance of benzene in the formation of PAHs, the formation mechanisms of interstellar benzene are not well understood. A single ion–molecule reaction sequence is considered when modelling the formation of benzene in the interstellar medium, beginning with the protonation of acetylene. Although this process has been used to model the initial steps in the formation of PAHs, it has not been experimentally measured. To explore this reaction mechanism, we have carried out an experimental study of sequential ion–molecule reactions beginning with protonation of acetylene under single-collision conditions. Surprisingly, we found that the reaction sequence does not result in benzene but, instead, terminates at  $C_6H_5^+$ , which is unreactive towards either acetylene or hydrogen. This result disproves the previously proposed mechanism for interstellar benzene formation, thus critically altering our understanding of interstellar PAH formation.

Aromatic molecules play a critical role in our understanding of the chemical evolution of the Universe<sup>1</sup>. About 10–25% of all interstellar carbon is assumed to be in the form of polycyclic aromatic hydrocarbons (PAHs), which are attributed to be the source of numerous broad infrared spectral features found throughout the interstellar medium (ISM)<sup>2</sup>. Although PAHs have long been inferred to be present in sizeable abundance in the ISM, recent observations by rotational spectroscopy at radio frequencies have definitively proven the existence of several aromatic molecules<sup>3–8</sup>. Benzene, the building block for all PAHs, has been observed in a variety of astronomical environments including planetary nebulae<sup>9</sup>, post-Asymptotic Giant Branch stars<sup>10</sup>, circumstellar envelopes of evolved carbon-rich stars<sup>11</sup>, and the comae of comets and asteroids<sup>12</sup>. Benzene has also been observed in the atmospheres of Saturn<sup>13</sup> and Titan<sup>14</sup> as well as in meteoritic chondrites<sup>15</sup>. Recent observations by the James Webb Space Telescope have revealed the presence of benzene and other smaller hydrocarbons in protoplanetary disks<sup>16,17</sup>. These observations have reinvigorated interest in interstellar benzene and PAHs because the formation mechanisms of PAHs throughout the ISM remain an open question. The exact mechanisms of PAH formation cannot be understood from astronomical observations alone. Instead, laboratory measurements are needed to supplement observations and

chemical models. To this end, we report an experimental mechanistic study of the sequential ion–molecule reactions starting with protonated acetylene and acetylene under single-collision conditions to identify a possible mechanism for the formation of benzene in the ISM.

The formation mechanisms of PAHs fall into two main categories: top-down mechanisms in which large interstellar clusters or large particles are fragmented by ultraviolet radiation to form PAHs<sup>18</sup> and bottom-up mechanisms in which small hydrocarbon molecules undergo a series of barrierless ion–molecule or radical–radical reactions to grow into large PAHs<sup>19–21</sup>. Although there is still an active debate over which mechanism is dominant in the context of the ISM, the bottom-up approach has received more attention due to the recent detection of PAHs, specifically in TMC-1 CP, a dark and diffuse starless cloud within the interstellar Taurus Molecular Cloud, where it is highly unlikely that PAH formation would be dominated by the degradation of large clusters or carbonaceous macromolecules<sup>4,22</sup>. Various experiments over the past decade have identified several possible bottom-up PAH growth mechanisms, including ion–molecule reactions, radical–radical reactions and radical–molecule reactions<sup>23–25</sup>. All these mechanisms begin with an already established aromatic molecule (one or more rings). Surprisingly, the formation of the first aromatic ring

<sup>1</sup>JILA, National Institute of Science and Technology and University of Colorado, Boulder, CO, USA. <sup>2</sup>Department of Physics, University of Colorado, Boulder, CO, USA. ✉e-mail: [stephen.kocheril@colorado.edu](mailto:stephen.kocheril@colorado.edu)

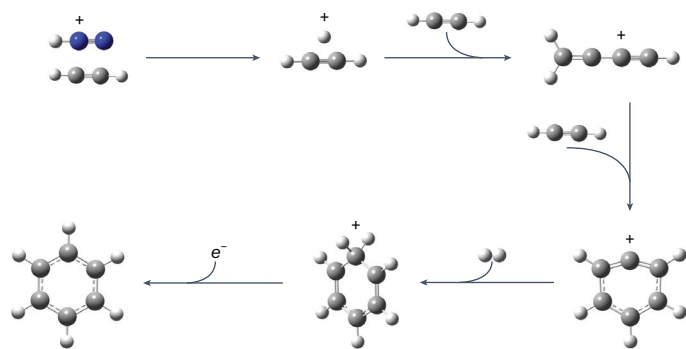


**Fig. 1 | Proposed synthesis mechanism for benzene in ion–molecule reactions.**

A proton donor (such as  $\text{N}_2\text{H}^+$ ) initiates the mechanism by protonating  $\text{C}_2\text{H}_2$  thereby forming  $\text{C}_2\text{H}_3^+$ .  $\text{C}_2\text{H}_3^+$  then reacts with  $\text{C}_2\text{H}_2$  to form  $\text{C}_4\text{H}_3^+$  through a condensation reaction.  $\text{C}_4\text{H}_3^+$  then undergoes a radiative-association reaction with  $\text{C}_2\text{H}_2$  to form  $\text{C}_6\text{H}_5^+$ .  $\text{C}_6\text{H}_5^+$  then undergoes a radiative-association reaction with  $\text{H}_2$  to form  $\text{C}_6\text{H}_7^+$ . Finally,  $\text{C}_6\text{H}_7^+$  undergoes electron recombination to form benzene.

has not received much experimental attention<sup>26</sup>. In bottom-up PAH formation mechanisms, the formation of the first aromatic ring (benzene) is widely considered to be both the limiting step of the process and the most difficult to probe experimentally<sup>24,26</sup>. Typically, astrochemical models must consider both radical–radical reactions and ion–molecule reactions if they are to accurately reproduce observed molecular abundances.

One primarily ion–molecule-based bottom-up mechanism has been considered for benzene formation throughout the ISM<sup>19,27</sup>, as shown schematically in Fig. 1. The reaction is initiated by the protonation of acetylene ( $\text{C}_2\text{H}_2$ ) by a proton donor, for example,  $\text{H}_3^+$ ,  $\text{N}_2\text{H}^+$  or  $\text{HCO}^+$ . The newly formed  $\text{C}_2\text{H}_3^+$  then reacts with another  $\text{C}_2\text{H}_2$  and undergoes a condensation reaction to form  $\text{C}_4\text{H}_3^+$ , which is followed by another addition of  $\text{C}_2\text{H}_2$  in a radiative-association-type reaction to form  $\text{C}_6\text{H}_5^+$ . It is assumed that the structure of  $\text{C}_6\text{H}_5^+$  is that of the deprotonated benzene cation (phenylium), which can undergo another radiative-association reaction with molecular hydrogen ( $\text{H}_2$ ) to directly form protonated benzene cation ( $\text{C}_6\text{H}_7^+$ ). Finally, protonated benzene can undergo electron recombination to yield neutral benzene. Although this mechanism has been included in chemical models<sup>19,27</sup>, this series of reactions has not been experimentally verified from start to finish. The reactivity of  $\text{C}_6\text{H}_5^+$ , specifically, has not been studied at low densities and temperatures, making it difficult to predict its reactivity in the ISM.

Previous experimental evidence supports the individual steps of this mechanism. Several types of ion–molecule reaction experiments have observed that sequential ion–molecule reactions of  $\text{C}_2\text{H}_2^+ + \text{C}_2\text{H}_2$  result in the formation of both  $\text{C}_4\text{H}_2^+$  and  $\text{C}_4\text{H}_3^+$  as primary products and both  $\text{C}_6\text{H}_4^+$  and  $\text{C}_6\text{H}_5^+$  as secondary products<sup>28–32</sup>. Additionally, several isomers of  $\text{C}_6\text{H}_5^+$  have been observed in these experiments. One isomer has been observed to be highly reactive with  $\text{C}_2\text{H}_2$  thereby forming  $\text{C}_8\text{H}_6^+$  and  $\text{C}_8\text{H}_7^+$ , and another isomer has been found to be unreactive. The observation of several isomers prompted an assignment of the unreactive isomer as the phenylium structure and the reactive isomer as an acyclic structure. The assignment of isomer structures was based on an energetics argument, as the cyclic isomer was known to be far lower in energy than the acyclic structure<sup>31,32</sup>.

The formation of a possible phenylium cation and its lack of reactivity has been of high interest to chemists generally. This led to several experiments with the express purpose of understanding both the structure and reactivity of the  $\text{C}_6\text{H}_5^+$  ion. These results were somewhat controversial, as several studies found that the assumed phenylium isomer of  $\text{C}_6\text{H}_5^+$  is unreactive<sup>33–35</sup>, whereas several others found that it is highly reactive with acetylene<sup>36–38</sup>,  $\text{H}_2$  (refs. 39–41) and

other hydrocarbons<sup>42–44</sup>. Several studies of collisionally induced dissociation also found that the structure of a  $\text{C}_6\text{H}_5^+$  fragment was highly dependent on the structure of the precursor molecule<sup>45</sup>. Recent studies on the fragmentation of substituted phenyl rings, such as phenylbromide or benzonitrile, observed  $\text{C}_6\text{H}_5^+$  to be one of the main products. The phenylium structure has been confirmed with infrared multi-photon dissociation<sup>46</sup>, vacuum ultraviolet photodissociation<sup>47</sup> and infrared pre-dissociation<sup>48</sup>. To our knowledge, there have been no spectroscopic studies on the cyclic isomer of  $\text{C}_6\text{H}_5^+$  formed through bottom-up synthesis.

All the previously mentioned reaction experiments were conducted at high pressures ( $10^{-6}$  Torr or higher) and most also at high collision energies ( $>1$  eV). These environments probably led to the variability in the perceived reactivity of the  $\text{C}_6\text{H}_5^+$  ion, as at higher pressures, collisional stabilization will lead to a greater abundance of higher energy structures, which are more reactive than the global minimum structure. High collision energies make it easier to break chemical bonds, thereby unknowingly overcoming reaction barriers. These pressures and collision energies far exceed those in the ISM, where densities are low enough that, effectively, termolecular interactions never occur. This means that our current understanding of aromatic ring formation is hindered by the incomplete experimental data. To refine the models of interstellar chemical reactions, especially bottom-up ion–molecule mechanisms, a new type of experimental system that mirrors the environment of the ISM is required.

Our experimental system can mimic the low-pressure and low-energy environment of the ISM by trapping and laser-cooling atomic ions in an ultra-high vacuum chamber (Fig. 2). To reach single-collision conditions and temperatures below 10 K, we used a linear quadrupolar Paul trap to confine and laser-cool  $\text{Ca}^+$  in a Coulomb crystal, which is a pseudo-crystalline structure formed by an ensemble of cold, trapped ions, as shown in the inset of Fig. 2. The cold  $\text{Ca}^+$  ions sympathetically cooled co-trapped molecular ions to

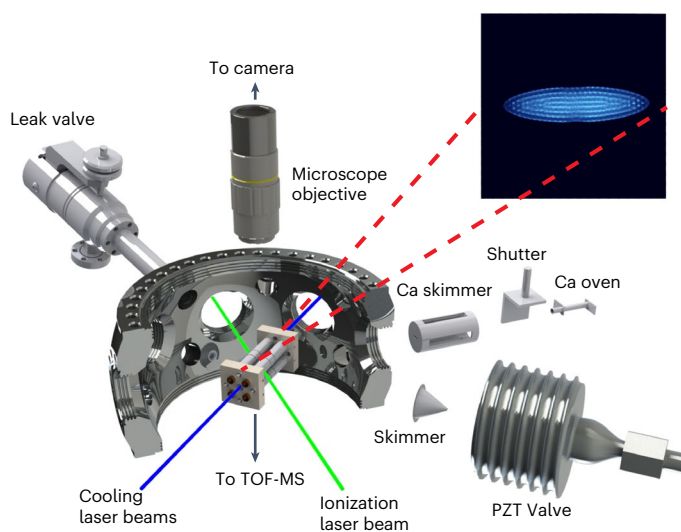


**Fig. 2 | Schematic of the experimental apparatus.** Cross-sectional view of the ultra-high-vacuum chamber showing the main components. An effusive  $\text{Ca}$  atomic beam was non-resonantly photoionized and the resulting ions were confined within a linear Paul trap. Molecular ions were loaded by resonantly photoionizing a skimmed molecular beam created by a piezoelectric transducer (PZT) valve. Fluorescence from laser-cooled  $\text{Ca}^+$  ions was imaged with an electron-multiplying charge-coupled device camera to provide a qualitative observation of reaction progression. Inset, example of such an image. Neutral reactants were admitted through the leak valve at a fixed pressure for variable amounts of time before the contents of the trap were ejected into the TOF-MS and detected using a set of microchannel plates in a chevron configuration. A new Coulomb crystal was loaded for each measurement. Figure adapted with permission from ref. 63, RSC.

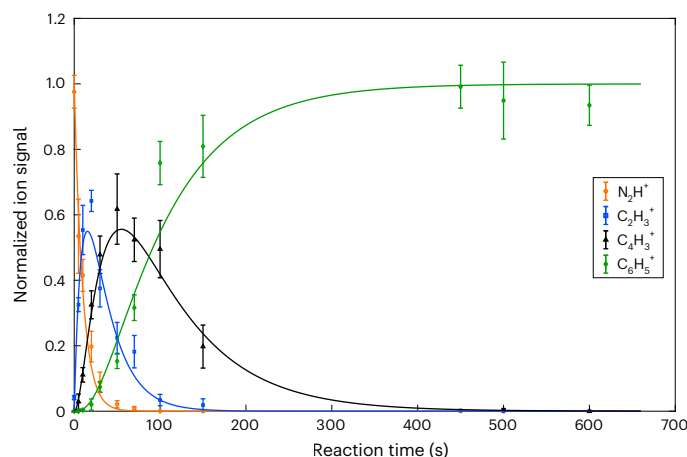


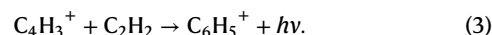
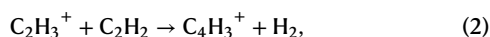
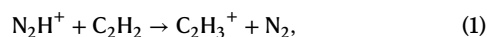
**Fig. 3 | Ion-reactant depletion and product growth for the sequential chain reactions starting with  $\text{N}_2\text{H}^+ + \text{C}_2\text{H}_2$ .** Experimental data points were fitted using a pseudo-first-order rate law (curves). Each data point corresponds to seven measurements and was normalized to the initial number of  $\text{N}_2\text{H}^+$  ions ( $\sim 90$ ). The orange circles corresponding to  $\text{N}_2\text{H}^+$  exhibit a sharp decay, which indicates the rapid reaction of the ions with  $\text{C}_2\text{H}_2$  to produce  $\text{C}_2\text{H}_3^+$ . As  $\text{C}_2\text{H}_3^+$  (blue squares) was produced, it reacted with another  $\text{C}_2\text{H}_2$  to form  $\text{C}_4\text{H}_3^+$ . The final reaction observed was  $\text{C}_4\text{H}_3^+$  (black triangles) reacting with another  $\text{C}_2\text{H}_2$  to produce  $\text{C}_6\text{H}_5^+$ . The  $\text{C}_6\text{H}_5^+$  signal (green diamonds) was observed to plateau over time, which indicates the termination of the chain reactions. All error bars represent the 68% confidence interval from the fit.

single-kelvin translational temperatures<sup>49</sup>. As the Coulomb crystal had an ion–ion spacing of  $\sim 10 \mu\text{m}$ , there was no collisional cooling of the vibrational or rotational modes of the co-trapped molecular ions. A detailed description of the apparatus is provided in Methods. Briefly, reactions were initiated by introducing the neutral reactant into the vacuum system at pressures that resulted in collision rates between the neutral acetylene and trapped ions of the order of one collision per second. This ensured that only two-body collisions occurred so that we did not need to consider the possibility of termolecular reactions or reactions with more bodies. As each reaction proceeded, all the ionic products were retained in the trap. We analysed the contents of the trap by ejecting all ions into a time-of-flight mass spectrometer (TOF-MS). By measuring the number of ions with each mass in the trap at different times, we could build kinetic reaction curves and determine the rates for each sequential reaction using a pseudo-first-order rate law, as the neutral  $\text{C}_2\text{H}_2$  was in excess. The low densities and temperatures of both the ion and neutral reactants allowed us to simulate conditions like that in the ISM and thus study both the mechanisms and the rates relevant to that environment. We found that the series of sequential reactions beginning with  $\text{C}_2\text{H}_3^+ + \text{C}_2\text{H}_2$  did not result in benzene but instead stopped at  $\text{C}_6\text{H}_5^+$ , which is unreactive for reactions with either  $\text{C}_2\text{H}_2$  or  $\text{H}_2$ . These results demonstrate that the established bottom-up mechanism for benzene formation does not actually produce benzene under single-collision conditions.

## Results

The series of ion–molecule reactions were initiated by the protonation of  $\text{C}_2\text{H}_2$ . The protonation of hydrocarbons by  $\text{N}_2\text{H}^+$  and other proton donors has been studied in detail previously<sup>50</sup>, and it is well understood that the protonation of  $\text{C}_2\text{H}_2$  by  $\text{N}_2\text{H}^+$  or even stronger acids like  $\text{H}_3^+$  results in the production of only  $\text{C}_2\text{H}_3^+$  (refs. 50,51).

The product growth observed for the chain reactions are shown in Fig. 3. The series of observed reactions are as follows:



$\text{N}_2\text{H}^+$  ( $m/z = 29$ ) reacted with neutral  $\text{C}_2\text{H}_2$ , which resulted in a reduction in the number of  $\text{N}_2\text{H}^+$  ions. The protonation of  $\text{C}_2\text{H}_2$  led to the formation of  $\text{C}_2\text{H}_3^+$  (equation (1)), as indicated by the rise of  $\text{C}_2\text{H}_3^+$  signal ( $m/z = 27$ ) at early times.  $\text{C}_2\text{H}_3^+$  then reacted with  $\text{C}_2\text{H}_2$  to form  $\text{C}_4\text{H}_3^+$  (equation (2)), as shown by the rise of the  $\text{C}_4\text{H}_3^+$  ion signal ( $m/z = 51$ ) and the decay of  $\text{C}_2\text{H}_3^+$ . The final reaction observed formed  $\text{C}_6\text{H}_5^+$  through reactions between  $\text{C}_4\text{H}_3^+$  and  $\text{C}_2\text{H}_2$  (equation (3)), as shown by the slow increase and plateau of the ion signal  $\text{C}_6\text{H}_5^+$  ( $m/z = 77$ ). The rates of each reaction were determined from the fits of each reaction set. The rate constants for each reaction are provided in Supplementary Table 1, along with comparisons to literature values and Langevin theory.

Although we were unable to probe the structures of the ions experimentally, we used quantum chemical calculations and previous spectroscopic work to infer the structures of the ions produced in the reactions and to construct the potential energy surfaces (see Supplementary Figs. 1 and 2 for details). Beginning with the primary product,  $\text{C}_2\text{H}_3^+$ , the structure has been probed in detail through spectroscopy in the infrared<sup>52,53</sup> and at millimetre and submillimetre wavelengths<sup>54</sup>. The structure has universally been found to be the ‘non-classical’ or bridged structure. Calculations also support the conclusion that this structure is the only energetically accessible structure in our experiments, so we assigned the  $\text{C}_2\text{H}_3^+$  structure to be the bridged structure. This reaction is shown in Fig. 4a.

The secondary product,  $\text{C}_4\text{H}_3^+$ , labelled as P3 in Fig. 4, has been studied in far less detail. Calculations have found that there are five possible structures for  $\text{C}_4\text{H}_3^+$  (ref. 55), but only the linear, protonated diacetylene structure was energetically accessible in our experiments, which is  $-0.68 \text{ eV}$  exothermic. The other computed structures were either endothermic by at least  $0.5 \text{ eV}$  or greater or had sizeable reaction barriers<sup>55</sup>. There have been two spectroscopic studies of  $\text{C}_4\text{H}_3^+$  isomers. One was carried out in He nanodroplets, and only the linear structure was observed<sup>56</sup>. The other was a study of infrared pre-dissociation<sup>48</sup> in which the linear structure of  $\text{C}_4\text{H}_3^+$  was observed as a dissociation fragment of benzonitrile. Considering both calculations and the spectroscopic data, we assigned the structure of  $\text{C}_4\text{H}_3^+$  as the protonated diacetylene structure.

The final tertiary product is  $\text{C}_6\text{H}_5^+$ , labelled P5 in Fig. 4. The  $\text{C}_6\text{H}_5^+$  cation has been the subject of several theoretical studies<sup>55,57,58</sup>. We carried out further calculations for possible isomers in our experiments. Over 30 possible isomers were energetically accessible in our experiment<sup>55,58</sup>. All spectroscopic analyses of  $\text{C}_6\text{H}_5^+$  have universally found the structure to be the phenylium structure, which is also the global minimum<sup>46–48</sup>. These spectroscopic studies were carried out by fragmenting substituted benzenes, such as benzonitrile, so it is difficult to conclusively say that the structure observed in those experiments is the same structure produced in our experiments because of the difference in formation mechanisms. However, our experimental evidence strongly indicates the presence of only the phenylium structure.

Radiative-association products, such as  $\text{C}_6\text{H}_5^+$ , are rare in single-collision experiments because most ions formed through highly exothermic reactions will readily break apart into smaller fragments in the absence of stabilizing collisions. In fact, even in the ion–molecule reaction studies that first observed  $\text{C}_6\text{H}_5^+$ , it was assumed that the ion was a collisionally stabilized complex<sup>28–32</sup>. However, our experiments were run under single-collision conditions, so that collisionally stabilized products were not possible. This means that the structure of the  $\text{C}_6\text{H}_5^+$  cation must be able to quench any internal energy by radiative relaxation, as the Coulomb crystal is only able to quench translational energy. Of all the computed structures, the phenylium structure seems most reasonable to be able to survive in the trap. Aromatic rings are known to be highly stable and resistant to fragmentation, as they have many vibrational modes that can dissipate energy through radiative

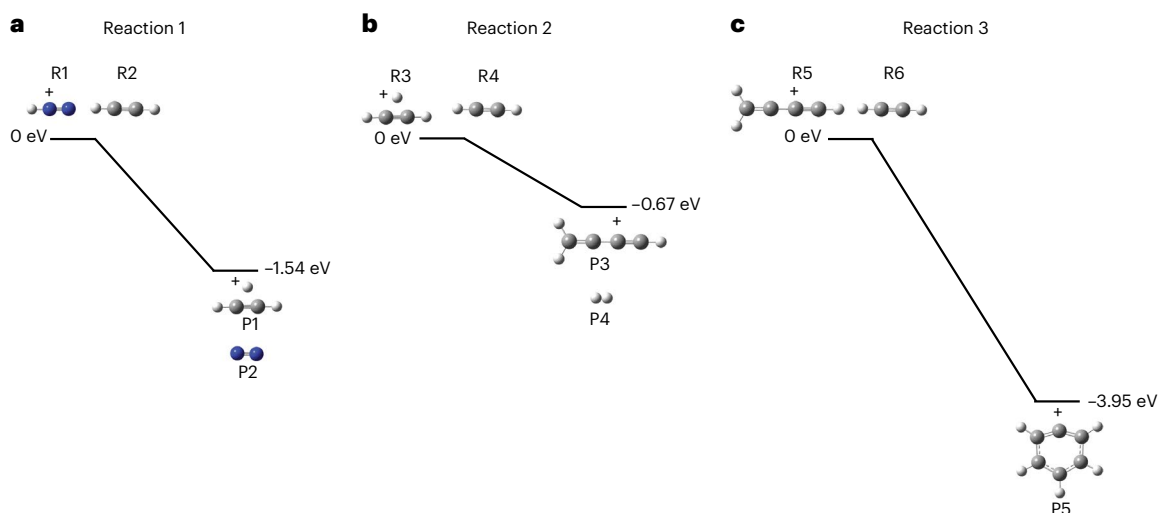


**Fig. 4 | Schematic diagram of the full series of sequential reactions.**

**a–c.** Only reactant and product states are shown for clarity. **a.** Reaction 1 shows the protonation of acetylene (R2) by  $\text{N}_2\text{H}^+$  (R1), which is calculated to be 1.54 eV exothermic. **b.** In reaction 2,  $\text{C}_2\text{H}_3^+$  (R3) reacts with  $\text{C}_2\text{H}_2$  (R4) and undergoes a condensation reaction to form  $\text{C}_4\text{H}_3^+$  (P3), which is calculated to be 0.67 eV

exothermic. **c.** In the final reaction, reaction 3,  $\text{C}_4\text{H}_3^+$  (R5) reacts with  $\text{C}_2\text{H}_2$  (R6) to form the final observed product  $\text{C}_6\text{H}_5^+$  (P5) through a radiative-association reaction, which is calculated to be 3.95 eV exothermic. Each reaction was computed at the MP2/aug-cc-pVTZ level of theory. The full potential energy surfaces for these reactions are shown in Supplementary Figs. 1 and 2.

relaxation instead of undergoing unimolecular decomposition<sup>55</sup>. Additionally, calculations have shown that the isomerization of  $\text{C}_6\text{H}_5^+$  from various structures to the phenylium structure was energetically feasible in our experiments<sup>55,58</sup>. As there were no collisions to prevent the isomerization process, it is highly probable that once any isomer of  $\text{C}_6\text{H}_5^+$  had formed, it would have quickly isomerized into the phenylium structure and then dissipated any excess internal energy through vibrational radiative relaxation before collisions with a neutral partner could occur.

Based on our results, astrochemical models are still missing crucial information needed to predict the formation of interstellar PAHs. Although our results closely follow the reaction mechanism shown in Fig. 1 up to the formation of  $\text{C}_6\text{H}_5^+$ , the lack of reactivity with acetylene does not address whether it is possible to form benzene using other neutral molecules. To further investigate the later steps of the proposed bottom-up mechanism, we carried out additional experiments in which  $\text{C}_6\text{H}_5^+$  was formed as described previously, but then instead of continuing to introduce acetylene, we introduced  $\text{H}_2$  into the trap to measure the reactivity of  $\text{C}_6\text{H}_5^+$  with  $\text{H}_2$ . Surprisingly, neither a depletion of  $\text{C}_6\text{H}_5^+$  nor the appearance of new mass channels was observed, indicating that  $\text{C}_6\text{H}_5^+$  did not react with  $\text{H}_2$ . The results of this reaction are shown in Supplementary Fig. 3. Our measurements put an upper bound on the reaction rate constant for  $\text{C}_6\text{H}_5^+$  with  $\text{H}_2$  to be  $\sim 1 \times 10^{-12} \text{ cm}^3 \text{ s}^{-1}$ . This upper limit is one order of magnitude higher than what has been measured previously and three orders of magnitude longer than the rate estimated from Langevin theory<sup>41</sup>. The reaction rate constants are summarized in Supplementary Table 1.

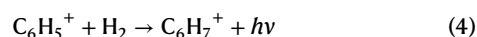
## Discussion and conclusions

Most of the ions present in this study have not been detected in the ISM. Only  $\text{C}_2\text{H}_3^+$  has been detected<sup>59</sup>, despite observations of both acetylene and benzene. Our results strongly indicate that each ion ( $\text{C}_2\text{H}_3^+$ ,  $\text{C}_4\text{H}_3^+$  and  $\text{C}_6\text{H}_5^+$ ) should be present throughout the ISM, particularly in regions with strong proton donors. Therefore, all the ions observed in this study should be high interest targets for high-resolution spectroscopy, either in the infrared or the microwave, to enable the astronomical detection of these ions. The observation or lack thereof of these ions in various regions of space will give crucial insights into the reactions occurring throughout the ISM, as  $\text{C}_6\text{H}_5^+$  could be a precursor to the formation of

astronomically observed aromatic molecules, such as benzonitrile or indene. Observing any or all of the product ions mentioned in our study would aid in improving astrochemical models, which in turn would improve our understanding of the chemical reactions occurring throughout space.

The observation of no reaction between  $\text{C}_6\text{H}_5^+$  and  $\text{H}_2$  is an important finding generally. Initial descriptions of the reactivity of the phenylium cation assumed it would be highly reactive because of the strong electrophilicity of the lowest unoccupied molecular orbital, a vacant non-bonding  $\sigma$  orbital (Supplementary Fig. 4), which induces  $sp$  hybridization of the lone C atom<sup>46,57</sup>. On the other hand, the electronic structure of  $\text{C}_6\text{H}_5^+$  does support it being highly stable and resistant to chemical reactions. The ground state has been described as a closed-shell  $^1\text{A}_1$  and as aromatic following Hückel's  $4n + 2$  electron counting rule. In fact, the same aromatic  $\pi$ -bonding orbitals of benzene are found in the phenylium, as outlined in Supplementary Fig. 4. As for benzene, it would be expected that phenylium would be highly stable and would react only with molecules that are able to activate the C–C bond, such as neutral radicals or anions, for example, strong nucleophiles. Previous reaction studies have been unable to ascertain which property, electrophilicity or aromaticity, is the driving force for the reactivity of phenylium, as the reactivity has been observed to vary depending on the experimental conditions<sup>33–44</sup>. However, our results clearly show that the stability enhanced by aromaticity is the dominant factor for the reactivity of phenylium, as no reaction occurred. This means that the formation mechanism shown in Fig. 1 is impossible under ISM conditions.

Note that the initial formation mechanism shown in Fig. 1 is correct up to the formation of  $\text{C}_6\text{H}_5^+$ . The sequence of reactions proceeds in a barrierless manner and the estimated rates of each reaction are in good agreement with our results. Additionally, calculations indicate that the reaction



is highly exothermic ( $>2 \text{ eV}$ ), which would complete the synthetic route to benzene after electron recombination<sup>19,27</sup>. Despite this, we observed that  $\text{C}_6\text{H}_5^+$  does not react with either acetylene or molecular hydrogen. This implies there are molecular dynamics determining the

reactivity and not simply energetics, as there is no barrier to reaction. The reactions of  $C_6H_5^+$  and other molecules should be of high interest to astrochemists broadly, especially dynamicists, as the exact details of the dynamics for the potential energy surface will probably hold the key to understanding this reaction and improving our understanding of chemical reactions between aromatic species, both terrestrial and interstellar. At present, it is clear that the formation of benzene does not occur through sequential ion–molecule reactions with acetylene, as the terminal product  $C_6H_5^+$  is a highly stable aromatic molecule that is unreactive towards either acetylene or hydrogen. Further studies are required to determine whether other bottom-up reactions might form benzene and, by extension, PAHs.

## Methods

### Experimental methods

Reactions were conducted in the ion trap apparatus previously described in ref. 49. The core of the apparatus is a linear quadrupolar Paul trap. An effusive beam of atomic Ca was produced by an oven source and directed to the centre of the ion trap, where it was non-resonantly ionized ( $\sim 7$  mJ per pulse, 355 nm, 10 Hz) to form  $Ca^+$ . As ions formed in the trap, they were laser-cooled to sub-kelvin temperatures ( $\sim 100$  mK) using the doubled output of a Ti-sapphire laser (MSquared SolisTiS,  $\sim 397$  nm, 2 mW) and an 866-nm diode laser (Toptica DLC Pro, 2 mW).  $Ca^+$  ions were used to sympathetically cool molecular ions to translational temperatures ranging from sub-kelvin to  $\sim 20$  K depending on the mass of the molecular ion. The ultra-high-vacuum chamber housing the ion trap had a background pressure of  $\sim 3 \times 10^{-10}$  Torr, as measured by a Bayard–Alpert ionization gauge. The number of ions in the trap was on average 1,400  $Ca^+$  ions and  $\sim 90$   $N_2H^+$  ions.

To generate the  $N_2H^+$  ions used to initiate the series of reactions,  $N_2^+$  ions were first loaded into the trap through a 2 + 1 resonance-enhanced multi-photon ionization scheme<sup>60</sup> ( $\sim 237$  nm, 0.7 mJ per pulse, 10 Hz). Once the  $N_2^+$  ions had been loaded into the trap, they were allowed to react with trace residual water in the vacuum chamber over the course of 2 min to form the  $N_2H^+$  used in this study. After this 2-min period had passed, a neutral acetylene (99.6% acetylene dissolved in acetone; Matheson Gas) mixture (20% in He) was introduced into the chamber through a pulsed leak valve for various reaction times. As the neutral gas was introduced at room temperature, the collision energies between the trapped ions and neutral gas were estimated to be between 150 and 230 K in the centre-of-mass frame. When the neutral gas was introduced, the total pressure was measured to be  $7.0 \pm 0.5 \times 10^{-9}$  Torr with a calculated partial pressure for  $C_2H_2$  of  $1.4 \pm 0.1 \times 10^{-9}$  Torr. After a predetermined reaction time, the valve was closed to end the reaction. The contents of the trap were sympathetically cooled for another 2 min before being ejected into the TOF-MS for product identification. All ions were considered to be vibrationally cold, as they had a full second to radiatively decay to the vibrational ground state. The rotational state distribution was assumed to be that for room temperature. Reaction curves were obtained by repeating this process for various reaction times ranging from 0 s to 10 min. Each time point was sampled at least seven times.

For the  $C_6H_5^+ + H_2$  reaction,  $C_6H_5^+$  was produced using the same procedure with a reaction time of 280 s. After the 2-min sympathetic cooling period, a neutral  $H_2$  (99.99%; Air Liquide) mixture (10% in He) was admitted into the chamber at a pressure of  $6.5 \times 10^{-8}$  Torr ( $6.3 \times 10^{-9}$  Torr partial pressure of  $H_2$ ). The reaction times were sampled between 0 and 300 s before the contents of the trap were ejected into the TOF-MS for product identification. This procedure was repeated at least four times for each reaction time.

### Theoretical methods

**Rate equations.** The reaction curve data were fitted using a least-squares curve fit and the following pseudo-first-order rate equations:

$$\frac{dN_{29}}{dt} = -k_1 N_{29}, \quad (5)$$

$$\frac{dN_{27}}{dt} = k_1 N_{29} - k_2 N_{27}, \quad (6)$$

$$\frac{dN_{51}}{dt} = k_2 N_{27} - (k_3 + k_4) N_{51}, \quad (7)$$

$$\frac{dN_{77}}{dt} = k_3 N_{51}, \quad (8)$$

where  $N_i$  corresponds to the number of ions observed at mass-to-charge ratio  $i$ , and  $k_i$  corresponds to the fitted value of the  $i$ th reaction rate constant of the sequential reactions.

The reaction rate constant  $k_4$  represents a contaminant protonation reaction occurring between the  $C_4H_3^+$  ions and trace amounts of acetone present in our acetylene cylinder. The only observed product involving acetone was protonated acetone ( $C_3H_7O^+$ ). This product formed after the production of  $C_4H_3^+$  and continued to grow until the  $C_4H_3^+$  ions had been depleted, and it remained in the trap for the duration of the reaction. As the total number of ions was conserved over the course of the reaction and as the ions maintained  $\sim 10$   $\mu$ m spacing in the Coulomb crystal, we concluded that this contaminant did not affect the reactivity of the main reactions with acetylene. As a result of this contaminant reaction, our data had to be normalized to the initial number of  $N_2H^+$  minus the amount of protonated acetone present at each time point.

Although no reaction products were observed in the reactions between  $C_6H_5^+$  and either  $C_2H_2$  or  $H_2$ , upper limits on the reaction rate constants for these reactions were determined by assuming that  $C_6H_7^+$  products were observed using the following pseudo-first-order rate equations:

$$\frac{dN_{77}}{dt} = -k_{\text{calc}} C_X N_{77}, \quad (9)$$

$$\frac{dN_{\text{prod}}}{dt} = k_{\text{calc}} C_X N_{77}, \quad (10)$$

where  $N_{\text{prod}}$  corresponds to the number of potential product ions from the reaction of  $C_6H_5^+$  with  $C_2H_2$  or  $H_2$ ,  $N_{77}$  corresponds to the number of  $C_6H_5^+$  ions,  $C_X$  is the concentration (molecules per  $\text{cm}^3$ ) of  $C_2H_2$  or  $H_2$ , and  $k_{\text{calc}}$  corresponds to the reaction rate constant for the reaction between  $C_6H_5^+$  and  $C_2H_2$  or  $H_2$ , depending on which reaction rate constant is being determined. This system of equations can be solved for  $k_{\text{calc}}$  to give the following equation:

$$k_{\text{calc}} = \frac{1}{t C_X} \ln \frac{N_{77}(0)}{N_{77}(0) - N_{\text{prod}}(t)}, \quad (11)$$

where  $t$  is the reaction time in seconds and  $N_{77}(0)$  is the initial amount of  $C_6H_5^+$  ( $\sim 90$  ions for the reaction with  $C_2H_2$  and  $\sim 45$  ions for the reaction with  $H_2$ ). Using both the pressures and reaction times mentioned previously along with an arbitrary signal of five product ions for  $N_{\text{prod}}(t)$ , which was well above the noise floor, yielded upper limits of  $\sim 4 \times 10^{-12} \text{ cm}^3 \text{ s}^{-1}$  and  $\sim 1 \times 10^{-12} \text{ cm}^3 \text{ s}^{-1}$  for the reactions with  $C_2H_2$  and  $H_2$ , respectively. Note that Bayard–Alpert ionization gauges have reduced accuracy below pressures of  $10^{-8}$  Torr (ref. 61). Therefore, the reaction rate constants that we obtained have some possible systematic uncertainty. The uncertainties provided represent statistical uncertainties in the measurements and do not reflect the accuracy of the ionization gauge.

**Quantum chemical calculations.** Possible potential energy surfaces for the series of reactions studied here were calculated at the unrestricted MP2/aug-cc-pVTZ level using the Gaussian 16 software package<sup>62</sup>. Each surface begins with the reactants at infinite separation and progresses from one stationary point to the next until the final products are obtained. Stationary points were identified through optimization and frequency calculations. The transition states, in particular, were identified by the presence of a vibrational mode with an imaginary frequency. Once a transition state had been found, the structure was altered along the direction of the imaginary-frequency vibrational mode and a subsequent stationary point was determined. Only barrierless pathways were considered because of the low-temperature environment of the experiment. The energy for each stationary point was corrected for the zero-point energy. The potential energy surfaces obtained from these calculations are provided in Supplementary Figs. 1 and 2. In addition to these surfaces, molecular orbitals for the phenylium structure were calculated, as shown in Supplementary Fig. 4. The three  $\pi$  bonding orbitals, outlined in the red boxes, indicate the presence of  $4n + 2$  Hückel aromaticity.

## Data availability

All data are available in the text or in the Supplementary Information. Source data are provided with this paper.

## References

- Allamandola, L., Boersma, C., Lee, T., Bregman, J. & Temi, P. PAH spectroscopy from 1 to 5  $\mu\text{m}$ . *Astrophys. J. Lett.* **917**, L35 (2021).
- Tielens, A. G. Interstellar polycyclic aromatic hydrocarbon molecules. *Annu. Rev. Astron. Astrophys.* **46**, 289–337 (2008).
- McGuire, B. A. et al. Detection of the aromatic molecule benzonitrile ( $c\text{-C}_6\text{H}_5\text{CN}$ ) in the interstellar medium. *Science* **359**, 202–205 (2018).
- McGuire, B. A. et al. Detection of two interstellar polycyclic aromatic hydrocarbons via spectral matched filtering. *Science* **371**, 1265–1269 (2021).
- Burkhardt, A. M. et al. Discovery of the pure polycyclic aromatic hydrocarbon indene ( $c\text{-C}_9\text{H}_8$ ) with GOTHAM observations of TMC-1. *Astrophys. J. Lett.* **913**, L18 (2021).
- Sita, M. L. et al. Discovery of interstellar 2-cyanoindene ( $2\text{-C}_9\text{H}_7\text{CN}$ ) in GOTHAM observations of TMC-1. *Astrophys. J. Lett.* **938**, L12 (2022).
- Cernicharo, J. et al. Pure hydrocarbon cycles in TMC-1: discovery of ethynyl cyclopropenylidene, cyclopentadiene, and indene. *Astron. Astrophys.* **649**, L15 (2021).
- Agúndez, M., Marcelino, N., Tercero, B. & Cernicharo, J. Aromatic cycles are widespread in cold clouds. *Astron. Astrophys.* **677**, L13 (2023).
- Cernicharo, J. et al. Infrared Space Observatory's discovery of  $\text{C}_4\text{H}_2$ ,  $\text{C}_6\text{H}_2$ , and benzene in CRL 618. *Astrophys. J.* **546**, L123 (2001).
- Kraemer, K. E. et al. A post-AGB star in the Small Magellanic Cloud observed with the Spitzer infrared spectrograph. *Astrophys. J.* **652**, L25 (2006).
- Malek, S. E., Cami, J. & Bernard-Salas, J. The rich circumstellar chemistry of SMP LMC 11. *Astrophys. J.* **744**, 16 (2011).
- Schuhmann, M. et al. Aliphatic and aromatic hydrocarbons in comet 67P/Churyumov–Gerasimenko seen by ROSINA. *Astron. Astrophys.* **630**, A31 (2019).
- Koskinen, T., Moses, J., West, R., Guerlet, S. & Jouchoux, A. The detection of benzene in Saturn's upper atmosphere. *Geophys. Res. Lett.* **43**, 7895–7901 (2016).
- Waite Jr, J. et al. The process of tholin formation in Titan's upper atmosphere. *Science* **316**, 870–875 (2007).
- Delsemme, A. The volatile fraction of the cometary nucleus. *Icarus* **24**, 95–110 (1975).
- Tabone, B. et al. A rich hydrocarbon chemistry and high C to O ratio in the inner disk around a very low-mass star. *Nat. Astron.* **7**, 805–814 (2023).
- Arabhavi, A. et al. Abundant hydrocarbons in the disk around a very-low-mass star. *Science* **384**, 1086–1090 (2024).
- Berné, O., Montillaud, J. & Joblin, C. Top-down formation of fullerenes in the interstellar medium. *Astron. Astrophys.* **577**, A133 (2015).
- Woods, P. M., Millar, T., Zijlstra, A. & Herbst, E. The synthesis of benzene in the proto-planetary nebula CRL 618. *Astrophys. J.* **574**, L167 (2002).
- Jones, B. M. et al. Formation of benzene in the interstellar medium. *Proc. Natl Acad. Sci. USA* **108**, 452–457 (2011).
- Pentsak, E. O., Murga, M. S. & Ananikov, V. P. Role of acetylene in the chemical evolution of carbon complexity. *ACS Earth Space Chem.* **8**, 798–856 (2024).
- Chabot, M., Béroff, K., Dartois, E., Pino, T. & Godard, M. Coulomb explosion of polycyclic aromatic hydrocarbons induced by heavy cosmic rays: carbon chains production rates. *Astrophys. J.* **888**, 17 (2019).
- Rap, D. B., Schrauwen, J. G., Redlich, B. & Bruünken, S. Noncovalent interactions steer the formation of polycyclic aromatic hydrocarbons. *J. Am. Chem. Soc.* **146**, 23022–23033 (2024).
- Kaiser, R. I. & Hansen, N. An aromatic Universe—a physical chemistry perspective. *J. Phys. Chem. A* **125**, 3826–3840 (2021).
- Bierbaum, V., Le Page, V. & Snow, T. PAHs and the chemistry of the ISM. *EAS Publ. Ser.* **46**, 427–440 (2011).
- Lee, K. L. K., McGuire, B. A. & McCarthy, M. C. Gas-phase synthetic pathways to benzene and benzonitrile: a combined microwave and thermochemical investigation. *Phys. Chem. Chem. Phys.* **21**, 2946–2956 (2019).
- McEwan, M. J. et al. New H and  $\text{H}_2$  reactions with small hydrocarbon ions and their roles in benzene synthesis in dense interstellar clouds. *Astrophys. J.* **513**, 287 (1999).
- Brill, F. W. & Eyley, J. R. Sequential ion–molecule reactions in acetylene. *J. Phys. Chem.* **85**, 1091–1094 (1981).
- Myher, J. & Harrison, A. Ion–molecule reactions in acetylene and acetylene–methane mixtures. *Can. J. Chem.* **46**, 1755–1762 (1968).
- Futrell, J. H. & Tiernan, T. O. Ionic reactions of unsaturated compounds. I. Polymerization of acetylene. *J. Phys. Chem.* **72**, 158–164 (1968).
- Anicich, V. G., Huntress Jr, W. T. & McEwan, M. J. Ion–molecule reactions of hydrocarbon ions in acetylene and hydrocyanic acid. *J. Phys. Chem.* **90**, 2446–2450 (1986).
- Knight, J., Freeman, C., McEwan, M., Anicich, V. & Huntress, W. A flow tube study of ion–molecule reactions of acetylene. *J. Phys. Chem.* **91**, 3898–3902 (1987).
- Eyley, J. R. & Campana, J. E. Gas-phase phenylium and acyclic  $[\text{C}_6\text{H}_5]^+$  isomers. *Int. J. Mass Spectrom.* **55**, 171–188 (1984).
- Giles, K., Adams, N. G. & Smith, D. A study of reactions of  $\text{C}_n\text{H}_m^+$  ions ( $n=4, 5, 6$ ;  $m=0-6$ ) with  $\text{H}_2$  and CO at 300K and 80K. *Int. J. Mass Spectrom.* **89**, 303–317 (1989).
- Contreras, C. S. & Salama, F. Laboratory investigations of polycyclic aromatic hydrocarbon formation and destruction in the circumstellar outflows of carbon stars. *Astrophys. J. Suppl. Ser.* **208**, 6 (2013).
- Fornarini, S. & Speranza, M. Is gaseous phenylium ion unreactive towards acetylene? *J. Chem. Soc. Chem. Commun.* **1985**, 1692–1693 (1985).
- Ausloos, P., Lias, S. G., Buckley, T. J. & Rogers, E. E. Concerning the formation and the kinetics of phenylium ions. *Int. J. Mass Spectrom.* **92**, 65–77 (1989).
- Soliman, A.-R. et al. Formation of complex organics in the gas phase by sequential reactions of acetylene with the phenylium ion. *J. Phys. Chem. A* **116**, 8925–8933 (2012).

39. Petrie, S., Javahery, G. & Bohme, D. K. Gas-phase reactions of benzenoid hydrocarbon ions with hydrogen atoms and molecules: uncommon constraints to reactivity. *J. Am. Chem. Soc.* **114**, 9205–9206 (1992).
40. Scott, G. B. et al.  $C_mH_n^+$  reactions with H and  $H_2$ : an experimental study. *J. Phys. Chem. A* **101**, 4973–4978 (1997).
41. Ascenzi, D. et al. Reactions of phenylium ions  $C_6(H, D)_5^+$  with  $D_2$ . *J. Chem. Phys.* **119**, 8366–8372 (2003).
42. Speranza, M., Sefcik, M. D., Henis, J. M. & Gaspar, P. P. Phenylium ( $C_6H_5^+$ ) ion-molecule reactions studied by ion cyclotron resonance spectroscopy. *J. Am. Chem. Soc.* **99**, 5583–5589 (1977).
43. Lifshitz, C., Gibson, D. & Levsen, K. Structure of the gas-phase ion  $C_6H_5^+$ . *Int. J. Mass Spectrom.* **35**, 365–370 (1980).
44. Ascenzi, D., Cont, N., Guella, G., Franceschi, P. & Tosi, P. New insights into the reaction mechanisms of phenylium ions with benzene. *J. Phys. Chem. A* **111**, 12513–12523 (2007).
45. Schröder, D., Schroeter, K., Zummack, W. & Schwarz, H. Charge inversion as a structural probe for  $C_6H_5^+$  and  $C_6H_6^+$  cations. *J. Am. Soc. Mass Spectrom.* **10**, 878–882 (1999).
46. Wiersma, S. D. et al. Ir photofragmentation of the phenyl cation: spectroscopy and fragmentation pathways. *Phys. Chem. Chem. Phys.* **23**, 4334–4343 (2021).
47. Jacovella, U. et al. Ultraviolet and vacuum ultraviolet photo-processing of protonated benzonitrile ( $C_6H_5CNH^+$ )—a plausible pathway to larger interstellar aromatics. *Astron. Astrophys.* **657**, A85 (2022).
48. Rap, D. B. et al. Fingerprinting fragments of fragile interstellar molecules: dissociation chemistry of pyridine and benzonitrile revealed by infrared spectroscopy and theory. *Faraday Discuss.* **245**, 221–244 (2023).
49. Schmid, P. C., Greenberg, J., Miller, M. I., Loeffler, K. & Lewandowski, H. J. An ion trap time-of-flight mass spectrometer with high mass resolution for cold trapped ion experiments. *Rev. Sci. Instrum.* **88**, 123107 (2017).
50. Milligan, D. B., Wilson, P. F., Freeman, C. G., Meot-Ner, M. & McEwan, M. J. Dissociative proton transfer reactions of  $H_3^+$ ,  $N_2H^+$ , and  $H_3O^+$  with acyclic, cyclic, and aromatic hydrocarbons and nitrogen compounds, and astrochemical implications. *J. Phys. Chem. A* **106**, 9745–9755 (2002).
51. Kim, J., Theard, L. & Huntress Jr, W. Reactions of excited and ground state  $H_3^+$  ions with simple hydrides and hydrocarbons: collisional deactivation of vibrationally excited  $H_3^+$  ions. *Int. J. Mass Spectrom.* **15**, 223–244 (1974).
52. Crofton, M. W., Jagod, M.-F., Rehfuss, B. D. & Oka, T. Infrared spectroscopy of carbo-ions. V. Classical vs nonclassical structure of protonated acetylene  $C_2H_3^+$ . *J. Chem. Phys.* **91**, 5139–5153 (1989).
53. Douberly, G. E. et al. Infrared photodissociation spectroscopy of protonated acetylene and its clusters. *J. Phys. Chem. A* **112**, 1897–1906 (2008).
54. Bogey, M., Cordonnier, M., Demuynck, C. & Destombes, J. Laboratory measurement of the millimeter and submillimeter wave spectrum of  $C_2H_3^+$ . *Astrophys. J. Lett.* **399**, L103–L105 (1992).
55. Peverati, R., Bera, P. P., Lee, T. J. & Head-Gordon, M. Insights into hydrocarbon chain and aromatic ring formation in the interstellar medium; computational study of the isomers of and their formation pathways. *Astrophys. J.* **830**, 128 (2016).
56. Moon, C. J. et al. Formation of the  $C_nH_n^+$  ( $n=2-5$ ) ions upon ionization of acetylene clusters in helium droplets. *J. Chem. Phys.* **158**, 224307 (2023).
57. Dill, J. D., Schleyer, P. R. & Pople, J. A. Molecular orbital theory of the electronic structure of molecules. 31. Substituent stabilization of the phenyl cation. *J. Am. Chem. Soc.* **99**, 1–8 (1977).
58. Shi, D. et al. Stability and isomerization reactions of phenyl cation  $C_6H_5^+$  isomers. *Chem. Phys.* **467**, 13–20 (2016).
59. Muller, S. et al. Protonated acetylene in the  $z=0.89$  molecular absorber toward PKS 1830-211. *Astron. Astrophys.* **683**, A62 (2024).
60. Opitz, S., Proch, D., Trickl, T. & Kompa, K. L. State-selective ionization of nitrogen by resonance-enhanced three- and four-photon excitation. *Chem. Phys.* **143**, 305–323 (1990).
61. Singleton, J. H. Practical guide to the use of Bayard–Alpert ionization gauges. *J. Vac. Sci. Technol. A* **19**, 1712–1719 (2001).
62. Frisch, M. J. et al. Gaussian 16 Revision C.01 (Gaussian Inc., 2016).
63. Schmid, P. et al. Isomer-selected ion–molecule reactions of acetylene cations with propyne and allene. *Phys. Chem. Chem. Phys.* **22**, 20303–20310 (2020).

## Acknowledgements

We thank L.-S. Wang and M.-A. Martin-Drummel for helpful discussions during the preparation of this manuscript. This work was supported by the National Science Foundation (Grant Nos. PHY-2317149 and CHE-1900294) and the Air Force Office of Scientific Research (Grant No. FA9550-20-1-0323).

## Author contributions

Data collection and analysis were carried out by G.S.K. and C.Z.-M. All authors contributed to interpreting the results and writing the manuscript.

## Competing interests

The authors declare no competing interests.

## Additional information

**Supplementary information** The online version contains supplementary material available at <https://doi.org/10.1038/s41550-025-02504-y>.

**Correspondence and requests for materials** should be addressed to G. S. Kocheril.

**Peer review information** *Nature Astronomy* thanks Brett McGuire and the other, anonymous, reviewer(s) for their contribution to the peer review of this work.

**Reprints and permissions information** is available at [www.nature.com/reprints](http://www.nature.com/reprints).

**Publisher's note** Springer Nature remains neutral with regard to jurisdictional claims in published maps and institutional affiliations.

Springer Nature or its licensor (e.g. a society or other partner) holds exclusive rights to this article under a publishing agreement with the author(s) or other rightsholder(s); author self-archiving of the accepted manuscript version of this article is solely governed by the terms of such publishing agreement and applicable law.

© The Author(s), under exclusive licence to Springer Nature Limited 2025